Proton-boron fusion scheme taking into account the effects of target degeneracy

S. J. Liu,[1] D. Wu,[2,*] T. X. Hu,[1] T. Y. Liang,[1] X. C. Ning,[1] J. H. Liang,[2] Y. C. Liu,[1] P. Liu,[1] X. Liu,[2] Z. M. Sheng,[1,†] Y. T. Zhao,[3] D. H. H. Hoffmann,[3] X. T. He,[1] and J. Zhang[2,4]

[1]*Institute for Fusion Theory and Simulation, School of Physics, Zhejiang University, Hangzhou 310058, China*

[2]*Key Laboratory for Laser Plasmas and School of Physics and Astronomy, and Collaborative Innovation Center of IFSA (CICIFSA), Shanghai Jiao Tong University, Shanghai 200240, China*

[3]*MOE Key Laboratory for Nonequilibrium Synthesis and Modulation of Condensed Matter, School of Physics, Xi'an Jiaotong University, Xi'an 710049, China*

[4]*Beijing National Laboratory for Condensed Matter Physics, Institute of Physics, Chinese Academy of Sciences, Beijing 100190, China*

(Received 7 June 2023; accepted 24 January 2024; published 25 March 2024)

The proton-boron (p-^{11}B) reaction is regarded as the holy grail of advanced fusion fuels, since the primary reaction produces three α particles with few neutrons and induced radioactivities from second order reactions. Compared to the deuterium-tritium reaction a much higher reaction temperature is required. Moreover, bremsstrahlung energy losses due to the high nuclear charge of boron deem it seemingly apparent than a fusion reactor based on deuterium-tritium plasma in equilibrium is to say the least very difficult. It is becoming more appealing to collide intense laser beams or accelerated proton beams with a boron target to produce p-^{11}B reactions. The fusion yield of p-^{11}B reactions is closely related to proton beam parameters and boron target conditions such as density, temperature, and ingredients. Degeneracy will increase fusion yields by reducing the stopping power of injected protons. In this work, we suggest a scheme for beam-target p-^{11}B fusions via injecting a MeV proton beam into a highly compressed quantum degenerated boron target. Such a boron target can be achieved via quasi-isentropic compression of solid boron by using precisely shaped laser pulses. Our results indicate that for densities ranging from 10^3 to $10^4\rho_s$, where ρ_s is the density of solid boron, contributions of bound and free electrons to the stopping of protons can be completely disregarded and dramatically reduced, respectively. The result is an increase in fusion yield by orders of magnitude. Furthermore, in order to achieve multiplication factor F greater than one, with F defined as the ratio of output fusion energy to the energy of injected protons, it is found there exists a minimum possible density of boron target, which is $1.8 \times 10^5\rho_s$ when the kinetic energy of injected protons is 880 keV.

DOI: 10.1103/PhysRevResearch.6.013323

I. INTRODUCTION

Apart from the advances in fusion research that made the headlines in public nonscientific journals, such as the record in confinement time at high temperature of the Hefei Experimental Advanced Superconducting Tokamak [1], the 59 megajoules of fusion power reported from the Joint European Torus in a Deuterium Tritium fusion experiment [1], and the burning plasma in an inertial fusion experiment from the National Ignition Facility of the Lawrence Livermore National Laboratory [1], there was a great number of more quiet achievements that demonstrate an accelerated pace towards the final goal of fusion energy [1–7]. While the mainstream of research and technological development is directed towards the deuterium-tritium reaction for fusion energy, the ^{11}B(p, α)2α process got renewed attention [8–10], since nonequilibrium conditions, as they are available in laser generated plasma, may turn out to be favorable to enhance the fusion yield [11]. The cross section of the ^{11}B(p, α)2α together with reactions like ^{12}C(e,e′p)^{11}B provides a direct probe for nuclear structure properties of ^{12}C [12–15]. Moreover, the abundance of ^{11}B in the universe is still an unresolved problem. Therefore, the investigation of these reactions will also contribute to solving the mystery of the low astrophysical abundances of the light elements Li, Be, and B in young main-sequence F and G stars [16,17]. Besides, the ^{11}B(p, α)2α reaction provides a method of cancer treatment [18].

Despite the recent progress, there is still a long way to go until fusion energy will finally be the solution to the global energy problem. All routes to fusion energy, as there are magnetic confinement fusion and inertial fusion, carry different inherent problems and at the moment it is not clear where the chances of success are highest. Therefore, all possible routes should presently be investigated thoroughly. However, there are not only technical problems or unsolved physics details, there is also the problem of supply of fusion fuel,

*dwu.phys@sjtu.edu.cn
†zmsheng@zju.edu.cn

especially tritium in the case of the DT-fusion reaction. The start of the ITER reactor in the 2030s will use the world's stockpile of tritium and it will take a while until tritium may be supplied by using fusion neutrons and lithium within the reactor. Therefore, we deem it important to investigate alternative routes using the ^{11}B(p, α)2α reaction. This reaction is a good candidate since the boron is readily available and neither in the entrance channel nor in the exit channel of the reaction radioactivity is involved [3]. There are of course reactions of second order, where neutrons are present and induced radioactivity may occur, but on a low and acceptable level [7]. Therefore, at government level in Europe a discussion started to license fusion power plants outside of the restrictions that are valid for fission power plants because it releases few radioactive products [18]. But there is a price to pay. The physical conditions to be met for fusion power based on proton boron fusion are much more demanding than those of DT. On the one hand, compared to the DT reaction, the p-^{11}B reaction requires more center-of-mass energy to reach its maximum nuclear reaction cross section and, on the other hand, radiation losses due to bremsstrahlung are overwhelmingly high and thus prevent a burning plasma in equilibrium conditions and equimolar fuel constituents, resulting eventually in no or very little net energy output [19,20]. However, with advances in high-intensity laser technology, the p-^{11}B fusion reactions using a PW-class laser in the "in-target" geometry or in the beam target ("pitcher-catcher") geometry are gradually becoming more attractive.

Based on this idea, a number of groups [10,11,23–31] have performed a series of experiments on p-^{11}B fusion reactions and measured the yields of α particles. The yields have been increased from about 10^5 sr^{-1} in 2005 [23,24] to about 10^{10} sr^{-1} in 2020 [28]. Giuffrida *et al.* [28] have investigated the p-^{11}B beam-target fusion reactions and calculated the fusion yields and Liu *et al.* [32] have also made a feasibility study of fusion reactors based on accelerators. Giuffrida *et al.* [28] previously addressed the role of the stopping power in a p-^{11}B fusion plasma that causes an elevation in fusion yield and especially they noted that the mass stopping power tends to decrease from ordinary matter to degenerate plasma. However, the stopping process of protons in detail has not been analyzed there, thus still leaving open ambiguities involving the interaction between the intense proton beams and the boron target. This interaction depends largely on the intensity of proton beams and the conditions of the boron target such as temperature, density, composition, and others. Beam intensity influences the stopping process as has recently been demonstrated [30]. The same is obviously true for the target and plasma parameters. It is important to uncover the relationship between these factors and their respective influence on the reaction probability. Among these factors, the degree of quantum degeneracy (also called degeneracy) is defined as $\Theta = T_F/T$ [33], in which the Fermi energy T_F and thermal temperature T are in eV. Electrons have to obey Fermi-Dirac statistics. For $\Theta \ll 1$ Boltzmann statistics may be applied.

In this paper, the quantitative relationship between the yields of p-^{11}B beam-target nuclear reactions and the density of boron targets is derived. By the way, the beam-target fusion reactions are similar to the in-flight fusion reactions [34]. We find that the effect of degeneracy will increase the fusion yields mediated by the effect of reducing the stopping power of the beam protons [35] under the situation of $\Theta \gg 1$ because, meanwhile, electrons must obey Fermi-Dirac statistics and the Pauli exclusion principle. We also verify that the fusion yields will increase when the boron target density is increased for the effect of degeneracy. Based on that, we suggest a different scheme for beam-target p-^{11}B fusions, where a MeV proton beam is injected into a highly compressed degenerated boron target. An outline of the suggested scheme is displayed in Fig. 1. A highly compressed degenerated boron target can be achieved via quasi-isentropic compression of a solid boron by using precisely shaped laser pulses [36,37]. For ideal gas, in an isentropic process, $T_2 = n^{1/(\gamma-1)}T_1$, where T_2 and T_1 are temperatures before and after the isentropic process, n is the density ratio after and before the isentropic process, and γ is the adiabatic coefficient. In this work, γ is set to 5/2, so $T_2 = n^{2/3}T_1$. Furthermore, the actual electron gas's Fermi energy T_F is proportional to $\rho^{2/3}$, where ρ represents the density of the Fermi electron gas. That is, $T \ll T_F$ could be maintained in an isentropic compression if the initial $T \ll T_F$ is guaranteed.

The radioactive losses for the degenerate medium are disregarded in this work because, on the one hand, the lower temperature of plasma will result in lower bremsstrahlung power and, on the other hand, the high density of plasma results in high radiation opacity [38]. Our results indicate that, for boron target of densities ranging from 10^3 to $10^4\rho_s$, contributions of bound and free electrons to the stopping of protons can be completely disregarded and dramatically reduced, respectively, which therefore results in orders of magnitudes increment of fusion yields. Furthermore, in order to achieve a multiplication factor F greater than one, we find that there exists a minimum required boron target density of $1.8 \times 10^5\rho_s$ when the kinetic energy of injected protons is 880 keV.

The structure of this paper is organized as follows. In Sec. II, a quantitative relationship between the reaction yields of p-^{11}B beam-target nuclear reactions as a function of proton stopping power per unit density is derived. In Sec. III, contributions from free electrons, bound electrons, and nuclei to the stopping power of protons are analyzed and compared with PIC simulations. In Sec. IV, in order to achieve multiplication with $F > 1$, the relation between the minimum possible density of compressed boron and the kinetic energy of injected protons is analyzed. Finally, discussions and conclusions are displayed in Sec. V.

II. BEAM-TARGET FUSION YIELDS

In general, to calculate the reaction yields of the proton-boron nuclear fusion, we first need to integrate the relative velocity distribution according to the cross section of the proton-boron nuclear fusion under the center-of-mass system to get the average reaction rate [36]

$$\langle \sigma v \rangle = \int_0^\infty \sigma(v) v f(v) dv, \tag{1}$$

where $f(v)$ is the distribution function of the relative velocities of protons to boron nuclei and $\sigma(v)$ is the corresponding cross section with v, which is the relative velocity of protons to boron nuclei. The number of reactions per unit time per

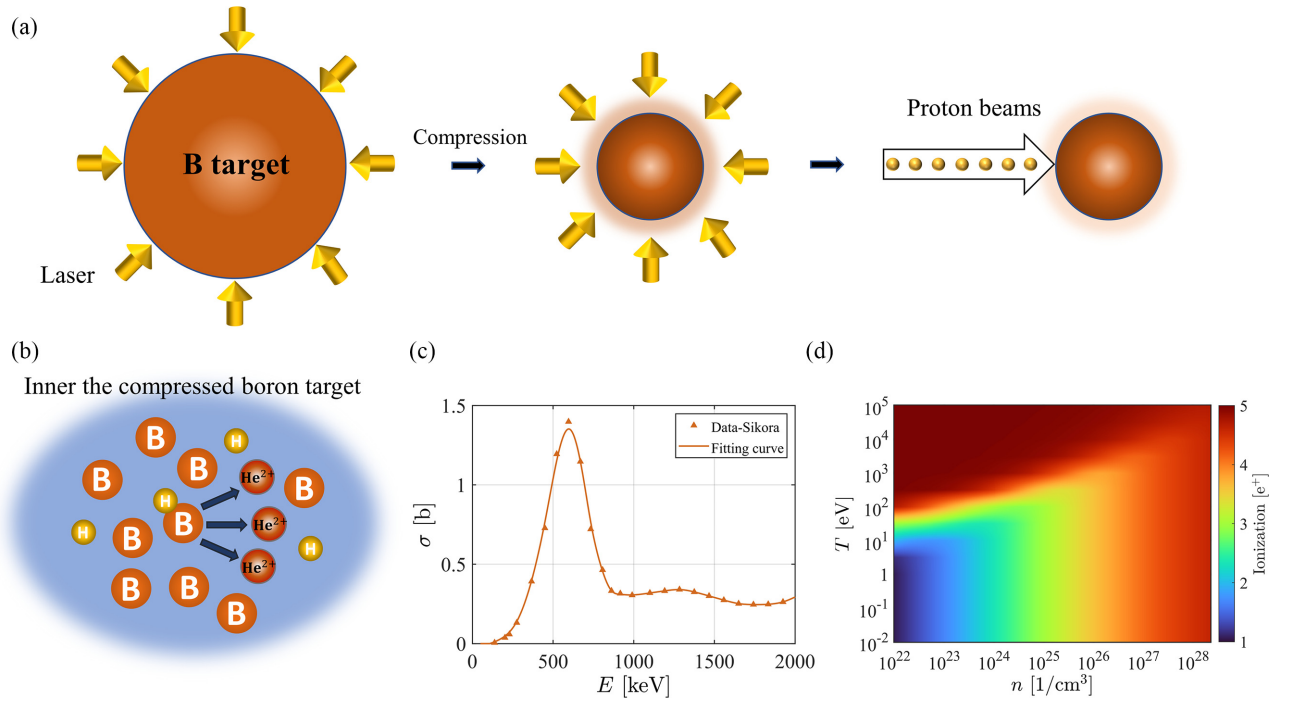

FIG. 1. (a), (b) Diagram of a p-^{11}B fusion scheme, (c) p-^{11}B fusion cross section as a function of center-of-mass energy, where the data of the orange triangle is extracted from the work of Sikora and Weller [21], and (d) The ionization degree of the boron target as a function of temperature and density of the boron target; the data is calculated by Heltemes's code BADGER [22].

unit volume, namely the volumetric reaction rate, is then calculated as $R = n_p n\langle\sigma v\rangle$, where n_p is the number density of protons and n is the number density of boron nuclei. It shows that the volumetric reaction rate is proportional to the density of protons and boron nuclei [36]. Finally, the total reaction number under a certain volume in a certain energy confinement time is obtained by multiplying R with the total volume and confinement time.

However, this method is strictly applicable only when the proton boron plasma is in thermal equilibrium. For nonequilibrium states, such as the process of projectile-target interaction, the relative velocity distribution changes rapidly. Therefore, the average reaction rate also changes with time. Here we propose a simple model to calculate the nuclear yields of beam-target reactions. In this model, we just consider the process of projectile-target interaction in p-^{11}B beam-target fusion while neglecting thermonuclear contributions. The previous work of Giuffrida [28] also proved that thermonuclear contributions to the fusion yields are negligible in the beam-target process. The density of incident protons is considered to be low; therefore, the action of the proton beam on the boron target can be regarded as a small perturbation. The temperature of the proton beam and boron target are kept at low levels, meaning that the relative velocities of protons and boron nuclei equal the injected velocities of the proton beam. Due to the interaction of the proton beam and boron target, when the protons move inside the boron target, they will be decelerated gradually.

We assume a small cloud of protons to be injected into the boron target and the proton number in this cloud is N_p. According to the proton energy, the deceleration process of this cloud inside of the boron target can be divided into many segments with infinitesimal volume and the energy of protons is considered constant within a respective segment. In the ith segment, the density of protons n_{pi} and the volume V_i will satisfy $N_p = n_{pi}V_i$. We only need to calculate the reaction number of every segment and sum them up. Then we will get the total reaction number during the deceleration process of protons.

During the deceleration process, the energy of protons has reduced from E_{pi} to $E_{pi} - \delta E_p$ in laboratory coordinates in the ith segment. The average reaction rate in the ith segment becomes $\sigma(v_i)v_i$ and then we can express the volumetric reaction rate in the ith segment as $R_i = n_{pi}n\sigma(v_i)v_i$. The reaction number in the ith segment during the time interval δt_i is $R_i\delta t_i V_i = nN_p\sigma(v_i)v_i\delta t_i = nN_p\sigma(E_{pi})\delta z_i$, where δt_i and δz_i are the deceleration time and the deceleration distance of the proton cloud in the ith segment, respectively, satisfying $\delta z_i = v_i\delta t_i$. We have

$$\delta z_i = \int_{E_{pi}}^{E_{pi}-\delta E_p} \frac{1}{dE/dx} dE, \tag{2}$$

where $dE/dx = -S$ and S is the stopping power of protons, which is also called the stopping force.

By integrating all segments, we can obtain the total reaction number as

$$R_T = nN_p \int_0^{E_p} \frac{\sigma(E)}{S} dE, \tag{3}$$

where $\sigma(E)$ is the p-^{11}B fusion cross section as a function of center-of-mass energy, as is shown in Fig. 1(c). The data of the orange triangle is extracted from the work of Sikora and Weller [21]. Equation (3) elucidates the relationship between

the number of reactions and the energy loss of protons in a boron target, which can be written into the form

$$R_T = N_p P = N_p \int_0^{E_p} \frac{\sigma(E)}{S/n} dE, \tag{4}$$

where P is the rate of a single proton triggering p-^{11}B nuclear reactions during the whole deceleration process and E_p is the initial energy of injected protons. A similar formula as Eq. (4) had also been derived by Giuffrida [28].

It is worth noticing that, since the cross section of the p-^{11}B fusion cannot be changed, P only depends on the stopping power per unit density $S_a = S/n$. Obviously, S_a is fully determined by the thermodynamic state (density and temperature) of the boron target [34,39–41].

III. STOPPING POWER OF PROTONS

Contributions to the stopping power of injected protons can be divided into three parts, i.e., stopping by collisions with free electrons, bound electrons, and nuclei. Generally speaking, the contribution from nuclear stopping is small unless at low incident energy. However, at highly compressed and quantum degenerate plasmas, the nuclear contribution cannot be ignored easily before a detailed analysis of the specific situation. In order to comprise all the three contributions, here we take the stopping power of protons as

$$S = S_f + S_b + S_n, \tag{5}$$

where S_f is from free electrons, S_b is from bound electrons, and S_n is from nuclei. As free and bound electrons contribute separately, to distinguish them, the ionization degree of the boron target with given density and temperature needs to be determined. According to the shielded hydrogen model and the single electron counting model [22], the ionization degree as a function of density and temperature is displayed in Fig. 1(d). The ions and electrons of the boron target are set to the same temperature T in this study. The data is calculated by Heltemes's code BADGER. For highly compressed and quantum degenerated (low temperature) plasmas, the degree of ionization depends only on the density. In our following analysis, the initial ionization state of the boron target is chosen according to Fig. 1(d).

A. Stopping contribution from free electrons

The stopping contribution from free electrons is closely related to degeneracy. To indicate the effect of degeneracy, here both theoretical analysis and computer simulations are displayed and compared to each other. We divide the part of theoretical analysis into semiclassical and quantum parts, respectively. Simulations are also divided into two parts: the classical part and the quantum part considering both Fermi-Dirac statistics and the Pauli exclusion principle.

As for the stopping contribution from free electrons, it was intensively analyzed with both the semiclassical partial wave scattering (SPWS) method [41–44] and the dielectric function method [39,45–49]. Within the dielectric formalism, the stopping power of a bare ion of mass $m_b \gg m_e$ and charge $Z_b e$ (m_e and e are the electron mass and the elementary charge, respectively) from free electrons moving with velocity v_p is given by [45,49,50]

$$S_f = \frac{2}{\pi}\left(\frac{Z_b e}{v_p}\right)^2 \int_0^\infty \frac{dk}{k} \int_0^{kv_p} d\omega\, \omega\, \mathrm{Im}\left(\frac{-1}{\varepsilon(\omega,k)}\right), \tag{6}$$

where $\varepsilon(k,\omega)$ is the complex dielectric function of the medium which depends on the wave number k and angular frequency ω of the electromagnetic disturbance caused by the bypassing projectile,

$$\varepsilon(\omega,\boldsymbol{k}) = 1 + \frac{4\pi}{k^2}\Pi_0(\omega,\boldsymbol{k}), \tag{7}$$

where $\Pi_0(\omega,\boldsymbol{k})$ is the free-electron density response function. The proportionality of S_f with Z_b^2 is a signature of linear-response theory. Semiclassically, the stopping contribution from free electrons that dismisses quantum wave effect can be derived from the Vlasov-Poisson equations

$$\left(\partial_t + \frac{\boldsymbol{p}}{m_e}\cdot\partial_r\right) f(\boldsymbol{r},\boldsymbol{p},t) + q\nabla\phi\cdot\partial_{\boldsymbol{p}} f(\boldsymbol{r},\boldsymbol{p},t) = 0 \tag{8}$$

and

$$\nabla^2\phi = -4\pi e\left[Z_b\delta(\boldsymbol{r}-\boldsymbol{v}_p t) - \frac{1}{m_e}\int d\boldsymbol{p}\, f + Zn\right]. \tag{9}$$

The δ function stands for the projectile ion moving with velocity $\boldsymbol{v}_p$. The last term in the Poisson equation represents the static plasma ion background. The f involved in the Vlasov-Poisson equations is Fermi-Dirac distribution. The semiclassical response function is

$$\Pi_0(\omega,\boldsymbol{k})_{sc} = -\int d\boldsymbol{p}\frac{\boldsymbol{k}\cdot\partial_{\boldsymbol{p}} f(\boldsymbol{p})}{\omega - \boldsymbol{k}\cdot\boldsymbol{v}}. \tag{10}$$

In quantum analysis, the stopping contribution from free electrons can be derived from the quantum-mechanical dielectric function method, which is also called the random-phase-approximation (RPA) method. With quantum wave effects, Wigner-Poisson equations [51,52] are usually used. It is convenient to replace the Vlasov equation with the Wigner equation,

$$\begin{aligned}\left(\partial_t + \frac{\boldsymbol{p}}{m}\cdot\partial_r\right) f(\boldsymbol{r},\boldsymbol{p},t) &= \frac{e}{i\hbar}\int d\boldsymbol{\xi}\int \frac{d\boldsymbol{p}'}{(2\pi\hbar)^3} e^{i(\boldsymbol{p}'-\boldsymbol{p})\cdot\boldsymbol{\xi}/\hbar} \\ &\times\left[\phi\left(\boldsymbol{r}+\frac{\boldsymbol{\xi}}{2}\right) - \phi\left(\boldsymbol{r}-\frac{\boldsymbol{\xi}}{2}\right)\right] f(\boldsymbol{r},\boldsymbol{p}',t).\end{aligned} \tag{11}$$

The f involved in the Wigner equation is Fermi-Dirac distribution. In this case the quantum response function is

$$\Pi_0(\omega,\boldsymbol{k})_q = -\int d\boldsymbol{p}\frac{f(\boldsymbol{p}) - f(\boldsymbol{p}+\hbar\boldsymbol{k})}{\hbar\omega - \boldsymbol{k}\cdot\hbar\boldsymbol{v} - \hbar^2k^2/2m}. \tag{12}$$

Taking the response function into $\varepsilon(\omega,k)$ and solving Eq. (6) numerically, we will obtain the stopping contribution from free electrons. Especially, in the limit of low projectile velocities, $v_p \ll v_{\mathrm{ave}}$, with v_{ave} the average electrons velocity, $v_{\mathrm{ave}} = (v_{th}^2 + v_F^2)^{1/2}$, where v_{th} is the thermal velocity of electrons and v_F is the Fermi velocity, the stopping contribution from free electrons is written as

$$S_f = \frac{4\pi Z_b^2 e^4 n_f}{m_e v_F^3} v_p \ln(\Lambda_f), \tag{13}$$

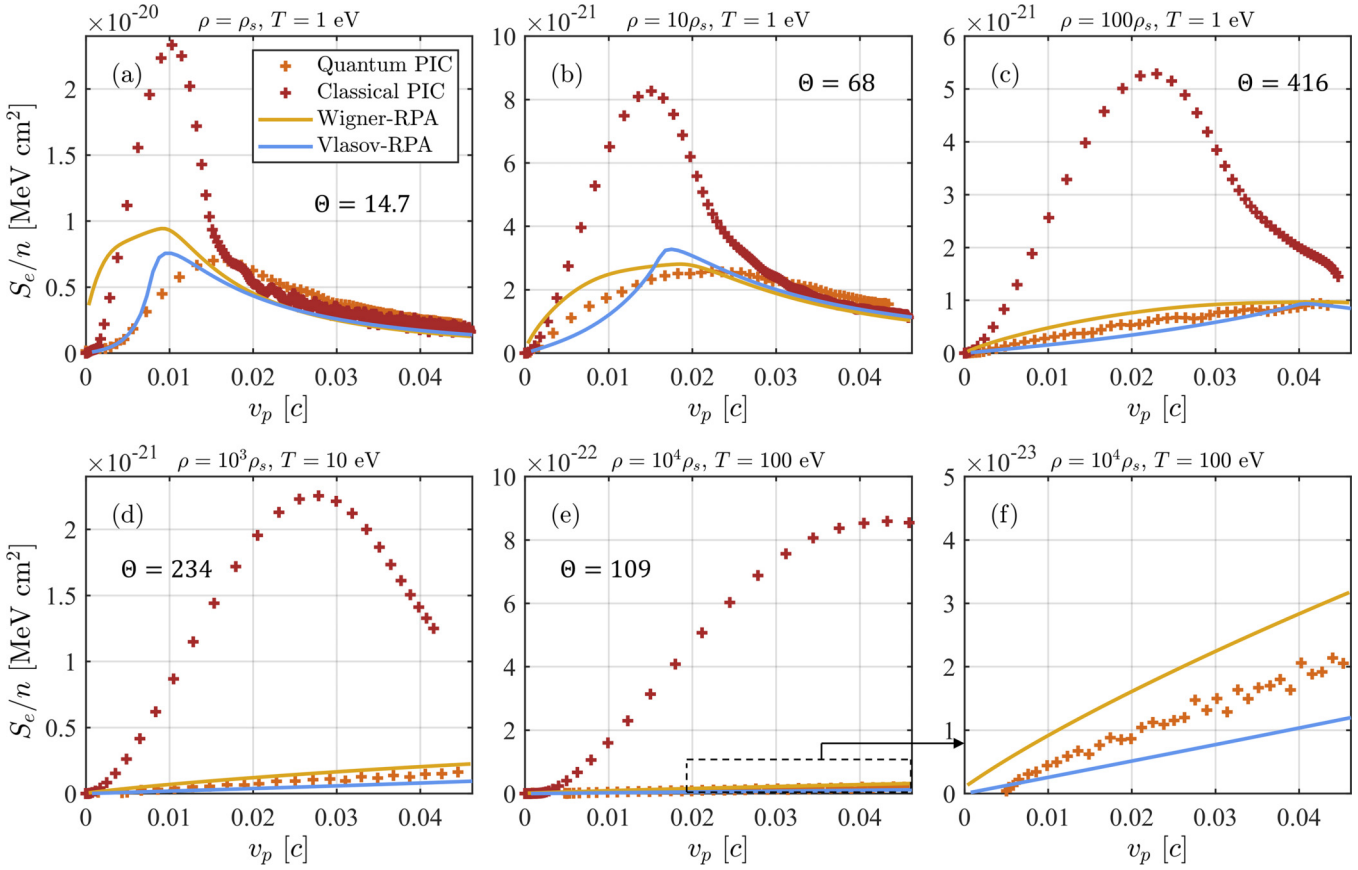

FIG. 2. Stopping power per unit density from free electrons as a function of densities and injected velocities of protons, where analytical results and values extracted from simulation by the LAPINS code are compared with each other, in which the analytical curves include "Wigner-Poisson" and the semiclassical "Vlasov-Poisson" methods and the numerical curves include values extracted from "Quantum PIC" and "Classical PIC" simulations.

where n_f is the number density of free electrons $n_f = Zn$ and $\ln(\Lambda_f)$ is the Coulomb logarithm, which changes little with the slowing down of protons. In the limit of high projectile velocities, $v_p \gg v_{\text{ave}}$, the stopping contribution from free electrons simplifies to [45]

$$S_f = \frac{4\pi Z_b^2 e^4}{m_e v_p^2} n_f \ln(\Lambda_f), \tag{14}$$

which already provides 1% accuracy for $v_p > 2v_{\text{ave}}$. See Appendix A for detailed information.

The statistic model used in the LAPINS code [53–56] to deal with the case that disregards degeneracy is based on the classical Boltzmann equation, where the average energy of electrons is only determined by the thermal temperature T. The model used in the LAPINS code to deal with degeneracy is based on the first principle Boltzmann-Uhling-Uhlenbeck (BUU) equation [57]. BUU collisions can ensure that the evolution of degenerate particles is enforced by the Pauli exclusion principle. This principle prevents degenerate particles from being scattered into an energy state that is already occupied. By using this code, we have simulated the stopping contribution from free electrons in different densities of the boron target. See Appendix B for relevant information.

In Fig. 2, the stopping power per unit density from free electrons S_e/n as a function of proton velocity is shown. The range of proton velocity considered is 0.001–0.0462c, with c the speed of light. The densities of the boron target in Figs. 2(a)–2(e) are respectively ρ_s, $10\rho_s$, $100\rho_s$, $10^3\rho_s$, and $10^4\rho_s$.

When we compare the cases disregarding and considering degeneracy in Fig. 2, i.e., "Classical PIC" and "Quantum PIC," we can find the effect of degeneracy does decrease the stopping power per unit density from free electrons S_e/n. The reason is due to the following two terms. First, as the most probable distribution of electrons is the Fermi-Dirac distribution, the average energy of electrons is much higher than the thermal temperature, which is

$$T_{\text{eff}} = T\left[\frac{2}{\sqrt{\pi}} F_{1/2}(\eta)(1+e^{-\eta})\right]^{2/3}, \tag{15}$$

where $F_{1/2}(\eta) = \int_0^\infty x^{1/2}(e^{x-\eta}+1)^{-1}dx$, $\eta = \mu/T$, and μ is the chemical potential. Second, the Pauli exclusion principle ensure that only electrons near the Fermi surface contribute to the stopping power, as those electrons deep inside the Fermi surface are frozen. Therefore, with the effect of degeneracy, the results of Quantum PIC indicate a decrease in S_e/n compared with those of Classical PIC under the same parameters of density and temperature.

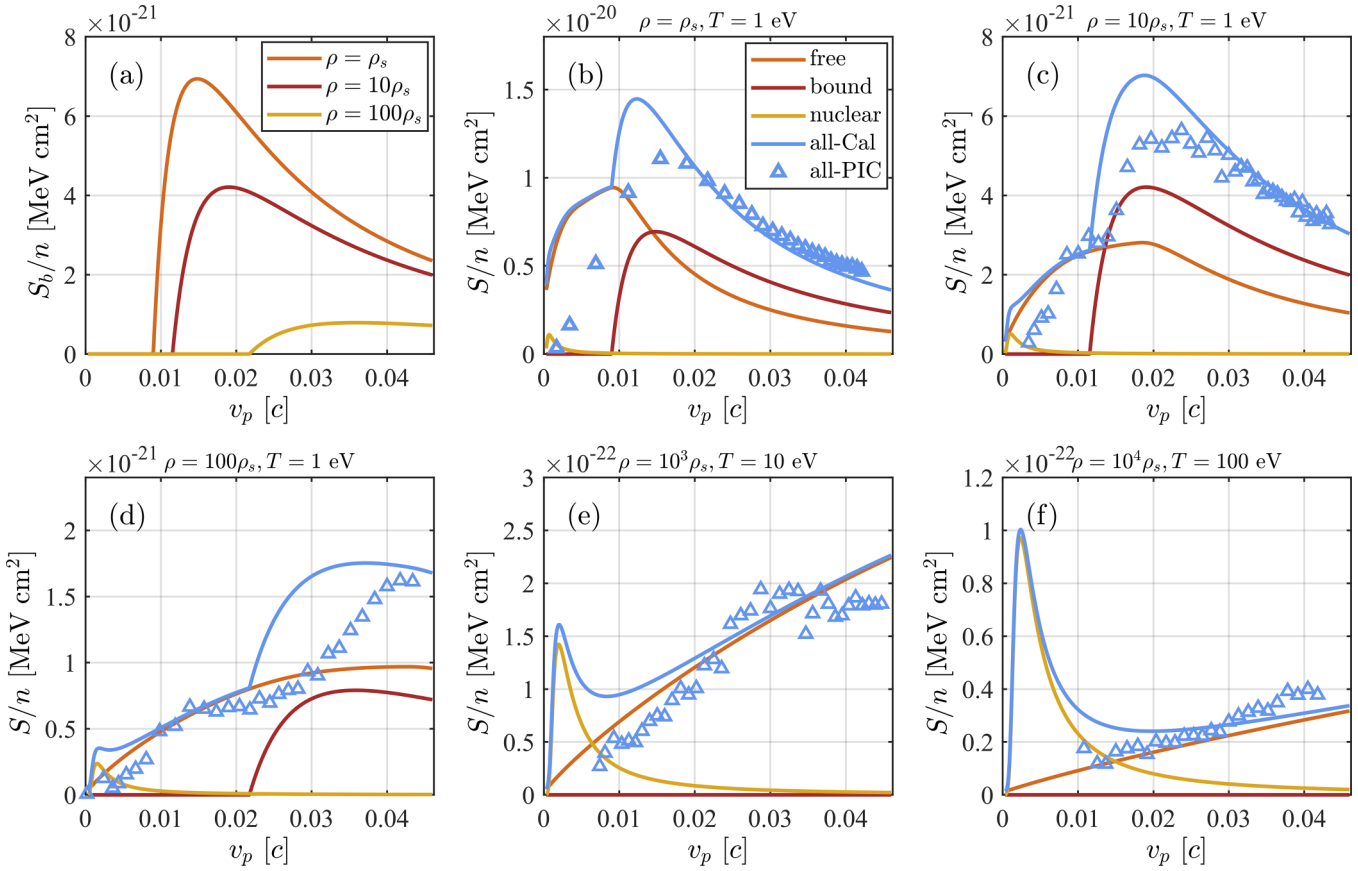

FIG. 3. (a) Bound electronic stopping power per unit density as a function of densities and velocities of injected protons. (b)–(e) The stopping power per unit density as a function of densities and velocities of injected protons, with contributions from the total, free electrons, bound electrons, and nuclei plotted, respectively. The label is shown in (b).

In the limit of low projectile velocities, the average electron stopping power S_e/n predicted by "Wigner-RPA" is proportional to the velocity of protons. In the limit of high projectile velocities, it is inversely proportional to the square of the velocity. It is shown that the results of Wigner-RPA and Quantum PIC agree with each other quite well. Due to the limitations of semiclassic stopping power theory, results of "Vlasov-RPA" depart from Wigner-RPA and Quantum PIC, but still show a similar trend. Especially, the result of Vlasov-RPA is well consistent with that of Wigner-RPA when the density of the boron target is lower than $100\rho_s$.

In addition, by analyzing the differences among the subpictures of Fig. 2, we find that, when the density of the boron plasma target is increased, the stopping contribution from free electrons per unit density decreases. This is because the effective temperature of free electrons is increased according to Eq. (15). Therefore, we can easily find the same trends hold for the cases of Quantum PIC, Vlasov-RPA, and Wigner-RPA, but not for the case of Classical PIC. This is because in the former three cases the Fermi-Dirac distribution is considered.

B. Stopping contribution from bound electrons

The model used in both analysis and LAPINS code to calculate the stopping contribution from bound electrons is based on the work of Fano [40], Trujillo [58], and Gil [59]. Generally, we can write the stopping contribution from bound electrons as

$$S_b = \frac{4\pi Z_b^2 e^4}{m_e v_p^2}(A - Z)n \ln(\Lambda_b), \tag{16}$$

where

$$\ln(\Lambda_b) \equiv \ln\left[\frac{2\gamma^2 m_e v_p^2}{\bar{I}(Z,A)}\right] - \beta^2 - \frac{C_K}{A} - \frac{\delta}{2}, \tag{17}$$

in which A is the atomic number of stopping medium, Z is the ionization degree of the background plasma, γ is the relativistic factor of the injected ions, and $\bar{I}(Z,A)$ is the average ionization potential considering the degeneracy effect [60,61]

$$\bar{I}(Z,A) = U - \bigtriangleup U + T_F, \tag{18}$$

with U the isolated ionization potential [62] and $\bigtriangleup U$ the ionization potential depression (IPD) [63]. As the density of the boron target is increased, the Fermi energy is also increased and ionizing the bound electrons needs to overcome an extra energy of T_F. In Eq. (17), the latter two terms are related to shell corrections and density effect corrections, respectively. These two terms are based on Fano's original work [40], to which the definitions of C_K/A and $\delta/2$ can be referred.

Figure 3(a) shows the stopping power per unit density from bound electrons S_b/n as a function of proton velocity during the deceleration process in different densities of the boron target. It is shown that S_b/n is decreased when the

density of the boron target is increased. Especially, it can be completely disregarded when the density of the boron target exceeds $100\rho_s$. Moreover, as the density of the boron target is increased, the average ionization potential $\bar{I}(Z, A)$ is increased as well, which is also reflected by the increasing peak positions of the stopping power per unit density from bound electrons when the density of the boron target is increased.

C. Stopping contribution from atomic nuclei

As for the stopping contribution from atomic nuclei, the typical binary collision method [64] is usually used,

$$S_n = \frac{4\pi Z_b^2 Z_t^2 e^4}{m_t v_p^2} n \ln(\Lambda_n), \tag{19}$$

where Z_t is the nuclear charge of the target particle, m_t is the mass of the target particle, and $\ln(\Lambda_n)$ is the Coulomb logarithm [65],

$$\ln(\Lambda_n) = \frac{1}{2}\left[\ln\left(1 + \frac{b_{\max}^2}{b_{\min}^2}\right) - \frac{b_{\max}^2/b_{\min}^2}{1 + b_{\max}^2/b_{\min}^2}\right], \tag{20}$$

with

$$b_{\min} = \frac{2Z_b Z_t e^2}{M_0 v_r^2}, \tag{21}$$

in which $M_0 = m_b m_t/(m_b + m_t)$ is the reduced mass, $b_{\min}$ represents the closest distance that two charged particles of the same sign, Z_b and Z_t, with relative velocity v_r, can reach, and $b_{\max}$ is an effective maximum impact parameter for nuclear collisions, with $b_{\max} = \max(\lambda_D, r_{WS})$. Due to the effects of high density and low temperature, the Debye length λ_D is usually smaller than the Wigner-Seitz radius $r_{WS} = (4\pi/3n)^{-1/3}$.

Figures 3(b)–3(e) show the contributions of all the three components (free electrons, bound electrons, and nuclei) to the stopping power per unit density of injected protons in the boron target. As can be seen in Fig. 3, at the low density region, S_n/n is far smaller than S_e/n and can be ignored. With the increasing of boron target density, the contribution of nuclei becomes important. Meanwhile, the peak of S_b/n moves to the right and the contribution of bound electrons dwindles. When the target density is 10^3-$10^4\rho_s$, the contributions of free electrons and nuclei determine the stopping power per unit density S/n, where S_e/n dominates at high proton velocity, while S_n/n dominates at low proton velocity.

IV. MULTIPLICATION FACTOR OF BEAM-FUSION REACTIONS

With the above analysis, we can easily obtain the total reaction number of beam-target nuclear fusion

$$R_T = N_p P = N_p \int_0^{E_p} \frac{\sigma(E)}{(S_f + S_b + S_n)/n} dE. \tag{22}$$

For the p-^{11}B beam-target reaction, the total number of reactions is closely related to the stopping power per unit density of protons in the target. As can be seen in Fig. 3, the total stopping power per unit density S/n decreases when the density of the boron target is increased. Especially when the density of the boron target reaches $10^3\rho_s$, S_b/n almost disappears, the total stopping power per unit density is now determined by

$$\frac{S}{n} = \frac{4\pi Z_b^2 Z_t^2 e^4}{m_t v_p^2} \ln(\Lambda_n) + \frac{4\pi Z_b^2 e^4 Z}{m_e v_F^3} v_p \ln(\Lambda_f). \tag{23}$$

The reason for the decrease is due to the following two facts. First, as $b_{\max}$ is inversely proportional to $n^{1/3}$, $\ln(\Lambda_n)$ decreases when the density of the boron target is increased. Second, as v_F^3 is proportional to $n_f = Zn$, the second term of Eq. (23) $\propto \ln(\Lambda_f)/n$ also decreases when the density of the boron target is increased.

Numerically, we have run simulations with different initial densities by using the LAPINS code, with density of ρ_s, $10\rho_s$, $100\rho_s$, $10^3\rho_s$, and $10^4\rho_s$, respectively. The initial kinetic energy of the proton beam is fixed at 1 MeV. Figure 4(a) shows the probability of the p-^{11}B beam-target fusion as a function of the boron target density. The comparisons between theoretical analysis and numerical simulations coincide with each other quite well. Due to a high degree of degeneracy, the effect of temperature is quite small on the reaction probability.

Quantitatively, it is critical to consider the energy multiplication factor F in order to achieve the net energy gain. Here F is a fundamental quantity in beam-target fusion [66],

$$F = \frac{P(E_p; n, T)Q}{E_p}, \tag{24}$$

where E_p is the initial proton energy and Q is the fusion Q value. For the p-^{11}B fusion reaction, Q equals 8.7 MeV. Theoretical analysis leads to the conclusion that, for injected protons of energy of 1 MeV, the threshold density of the boron target is $1.95 \times 10^5\rho_s$, beyond which the energy multiplication factor F would be greater than one.

Moreover, the cross section of nuclear fusion depends on the center-of-mass energy, which is a function of the injected proton energy. Therefore, different injected energy of proton beams may lead to different reaction probabilities. We have calculated the fusion probability with varying injected proton kinetic energies. In order to make the F factor more than one, we find, when the energy of injected protons is around 880 keV, there exists a minimum possible compressed density, which is $1.8 \times 10^5\rho_s$, as shown in Fig. 4(b).

By utilizing the ideal gas equation of state and taking into account the Fermi energy, we can estimate the total laser energy required,

$$\begin{aligned} E_L &= E_{Ln} + E_{Lp} \\ &= \frac{nV}{\eta_1}\left[(Z+1) \times \frac{3}{2}T + Z \times \frac{3}{5}E_F\right] + \frac{N_p E_p}{\eta_2}, \end{aligned} \tag{25}$$

where E_L is the total laser energy, E_{Ln} is the laser energy to compress the target usually by a nanosecond laser, and E_{Lp} is the laser energy to accelerate protons usually by a picosecond ultraintense ($>10^{18}$ W cm^{-2}) laser [67]. The energy conversion efficiency of compression and acceleration is η_1 and η_2, respectively. According to the work of Hey [68] and Robson [67], the conversion efficiency from laser energy into proton kinetic energy is about 5%. The conversion efficiency from laser energy to compressed target is 10%–33% [36].

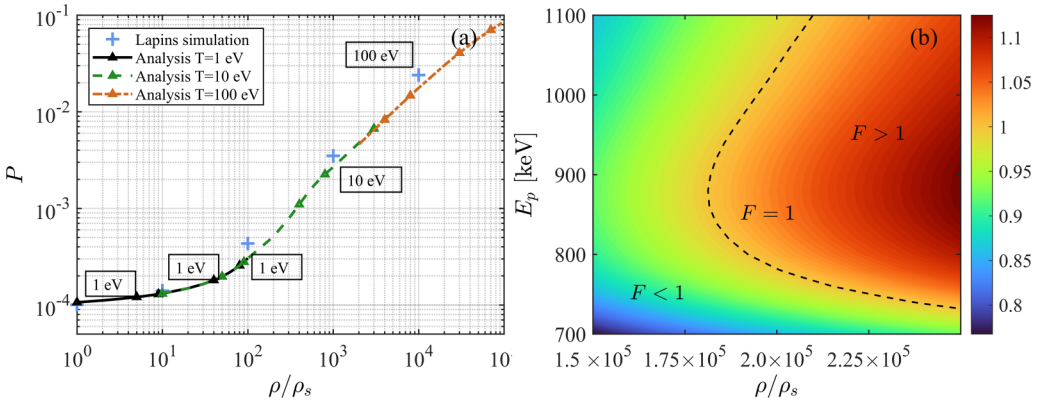

FIG. 4. (a) Reaction probability of the p-^{11}B nuclear fusion as a function of boron target density. The initial energy of the proton beam is 1 MeV. (b) The multiplication factor F of p-^{11}B beam-target fusion as a function of boron target density and initial proton kinetic energy. F is defined as the ratio of the fusion energy produced during the deceleration of the proton beam to the overall energy of injected protons.

When considering the energy of laser, the G factor of yield-to-laser energy can be rewritten as

$$G(E_p; n, T) = \frac{N_p P(E_p; n, T) Q}{E_L}. \tag{26}$$

In this study, because we do not take into account the impact of proton beam density, target composition, and other parameters that affect ignition, the G factor is substantially smaller than the F factor.

V. DISCUSSIONS AND CONCLUSIONS

It is worth mentioning that the present work assumes low density of a proton beam, so that the protons do not perturb the compressed boron plasma. Because the density of the proton beam is far lower than the density of the boron target and the range of the duration of the proton beam in our simulations is just set to 0.3–3 ps, the heating effect is not obvious in the boron medium. Since we do not consider the ignition currently and this work is more about the physical exploration of the beam-target p-^{11}B nuclear reaction process in a degenerate target, we cannot get a fusion-burning wave in the degenerate medium.

However, a dense beam with the parameters achieved by experiment is required in a practical scheme. In this case, the dense proton beam would heat the boron plasma and the degeneracy of the heating region would decrease. We simply

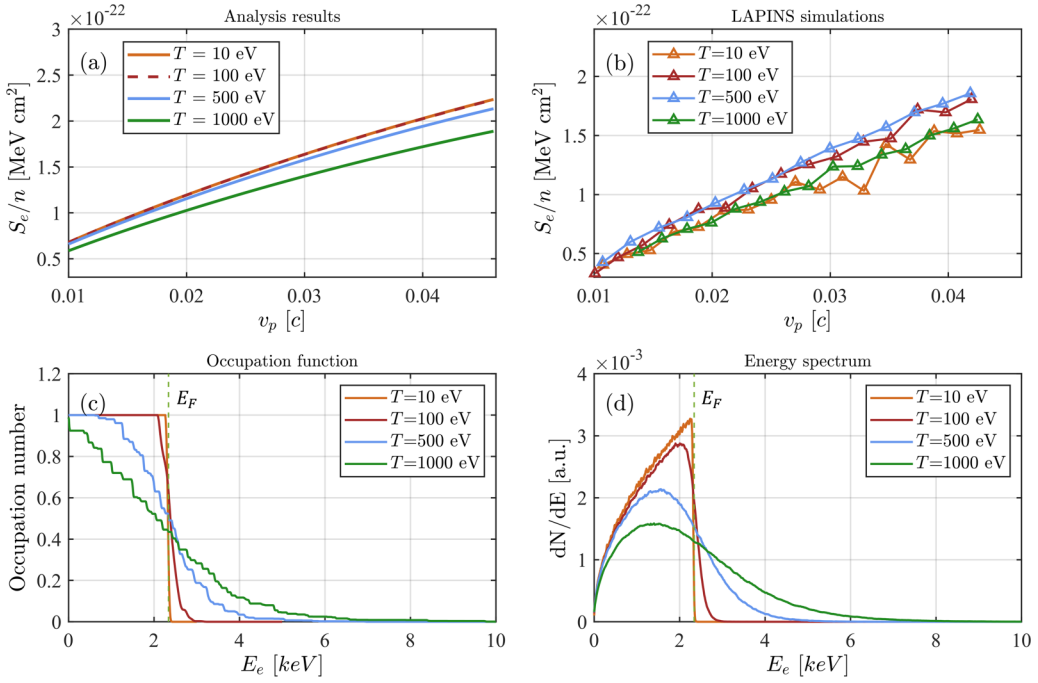

FIG. 5. (a) S_e/n as a function of the velocity of protons at different target temperatures with the target density $10^3\rho_s$ in theory. (b) S_e/n as a function of the velocity of protons at different target temperatures with the target density $10^3\rho_s$ in simulation. (c) The local occupation number of electrons in initial time as a function of energy of electrons in simulation. (d) The energy spectrum of electrons at different target temperatures with the target density $10^3\rho_s$ in simulation.

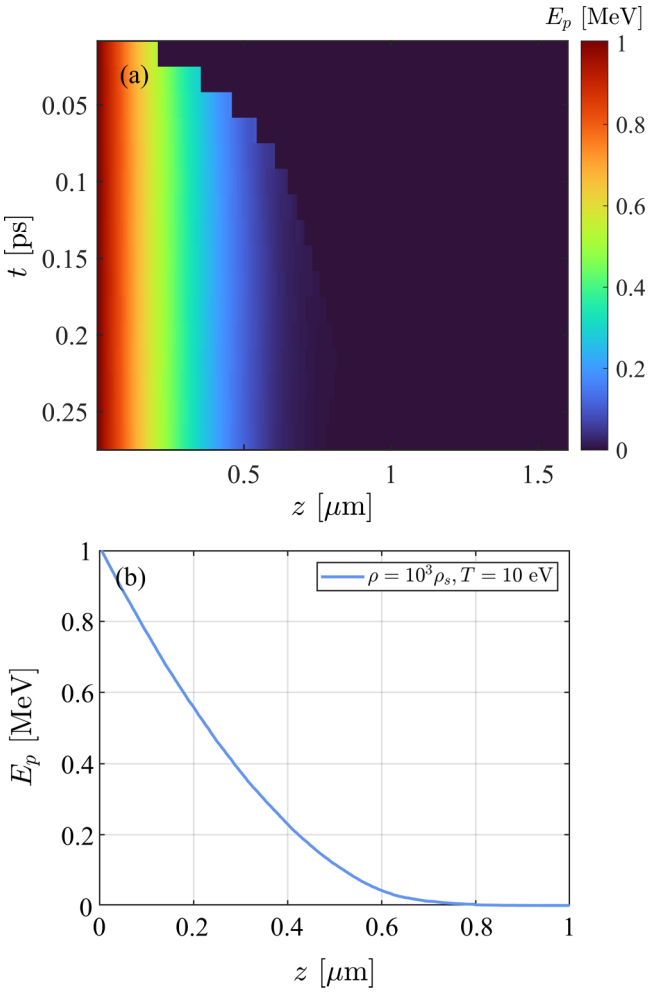

FIG. 6. (a) Proton energy as a function of time and incident distance, simulated by the LAPINS code considering the Pauli exclusion principle, with boron density of $10^3\rho_s$ and temperature of 10 eV. The duration of the beam is set long enough to ensure that the beam is still injected when the protons in the front are stopped. We therefore can get stable data describing the proton energy as a function of the incident distance during the deceleration process. (b) The proton energy as a function of the incident distance during the deceleration process.

consider the interaction of a proton beam with a boron target at different temperatures.

Theoretically, when the temperature of the interaction region is increased, though the degeneracy of the heating region is decreased, S_e/n would be decreased also, as is shown in Fig. 5(a), which can be seen in the Fig. 6 in Ref. [69] as well. This is because the interaction between protons and plasma does not take the Pauli exclusion principle into account. However, the LAPINS code has integrated the Pauli exclusion principle self-consistently; consequently, the simulations give forth a different result on S_e/n when the temperature of the boron target T is increased. Figures 5(b)–5(d) illustrate that, when the temperature of the target rises from 10 eV to 100 eV, S_e/n increases. At this point, the change in the distribution function causes electrons within the Fermi surface to be excited more easily. As the temperature rises to 500 eV, the impact of the average energy becomes equally significant to that of the Pauli exclusion principle. Finally, the thermal energy of electrons is comparable to Fermi energy, the Pauli exclusion principle acts weakly, and the average energy mainly accounts for the result that S_e/n decreases when T rises from 500 eV to 1000 eV.

In further study, the relevant physical processes described above will be taken into consideration and the effect of the heating process caused by an intense proton beam on the beam-target nuclear fusion yield will be quantitatively analyzed, which is also included in our LAPINS code.

Besides, instabilities are not considered in this work because of the extremely high density and relatively low temperature of the target. However, when we take the dense beam into consideration as well as the heating process, some collective instabilities may occur [70], which deserve further studies.

In addition, compression by a factor of 10^5 can hardly be achieved with presently known techniques [71]. However, when considering the heating process, the requirements may be reduced. In reality, in order to verify the results of this paper, as a first step, several hundred times the solid density would be sufficient in the experiment.

In conclusion, we suggest a scheme for beam-target p-^{11}B fusions via injecting a MeV proton beam into a highly compressed quantum degenerated boron target. The degeneracy effect is found to have an effect on the number of fusion reactions by decreasing the stopping power per unit density of protons in the boron target. At low boron target densities, free electrons and bound electrons dominate the stopping power per unit density. Especially when $E_p = 1$ MeV and $\rho = 10^3 - 10^4\rho_s$, S_b/n and S_e/n can be completely disregarded and dramatically reduced, respectively, which therefore results in orders of magnitude increments in fusion yields. When the injected proton beam has an energy of around 880 keV, there exists a minimum possible compressed density, which is $1.8 \times 10^5\rho_s$, to make the F factor greater than one.

ACKNOWLEDGMENTS

This work was supported by the Strategic Priority Research Program of Chinese Academy of Sciences (Grant No. XDA250050500), the National Natural Science Foundation of China (Grants No. 12075204, No. 11875235, and No. 61627901), and Shanghai Municipal Science and Technology Key Project (Grant No. 22JC1401500). D.W. acknowledges the sponsorship from Yangyang Development Fund.

D.W. initiated this work. S.J.L. performed the simulation and data analysis. S.J.L., D.W., and D.H.H.H. drafted the manuscript. All the author contributed to physical analysis.

APPENDIX A: CALCULATION OF THE STOPPING CONTRIBUTION FROM FREE ELECTRONS BY WIGNER-RPA EQUATIONS

Considering a homogeneous free electrons gas (FEG) with density n_f and Fermi wave number $k_F = (3\pi^2 n_f)^{1/3}$, the FEG can be characterized by the Lindhard parameter χ^2; these dimensionless quantities are linked to k_F through [45,49]

$$\chi^2 = (\pi k_F a_0)^{-1}, \tag{A1}$$

where $a_0 = \hbar^2/m_e e^2$ is the Bohr radius ($\hbar$ is the reduced Plank constant) and $\alpha = (4/9\pi)^{1/3}$. It is convenient to replace k and ω by the dimensionless variables

$$z = \frac{k}{k_F}, \quad u = \frac{\omega}{k v_F}, \tag{A2}$$

where $v_F = \hbar k_F/m_e$ stands for the Fermi velocity. In this case the dielectric function can be written as [49]

$$\varepsilon(z,u) = 1 + \frac{\chi^2}{z^2}[f_1(z,u) + i f_2(z,u)], \tag{A3}$$

with

$$f_1(u,z) = -\frac{\pi}{8z\Theta}[F(u+z) - F(u-z)]. \tag{A4}$$

When $\Theta \gg 1$,

$$F(p) = 2p\left[\frac{1}{2} + \frac{1-p^2}{4p}\ln\frac{p+1}{p-1}\right] \tag{A5}$$

and

$$f_2(u,z) = -\frac{\pi}{8\Theta z}\ln\frac{1+\exp[\mu/T - \Theta(u+z)^2]}{1+\exp[\mu/T - \Theta(u-z)^2]}. \tag{A6}$$

The stopping contribution from free electrons can be written in the form

$$S_f = \frac{4\pi Z_b^2 e^4}{m_e v_p^2} n_f L_e, \tag{A7}$$

with

$$L_e = \frac{6}{\pi\chi^2}\int_0^{v_p/v_F} u\,du \int_0^{\infty} z\,dz\ \mathrm{Im}\,\frac{1}{\varepsilon(z,u)}, \tag{A8}$$

which depends on the number density and temperature of target nuclei as well as the velocity of protons, satisfying

$$L_e = \left(\frac{v_p}{v_r}\right)^3 \ln(\Lambda_f). \tag{A9}$$

Here v_r is the relative velocity between protons and free electrons and $v_r = (v_{\mathrm{ave}}^2 + v_p^2)^{1/2}$. In the limit of low projectile velocity, $v_p \ll v_{\mathrm{ave}}$, Eq. (A9) becomes

$$L_e = \left(\frac{v_p}{v_r}\right)^3 \ln(\Lambda_f) \simeq \left(\frac{v_p}{v_F}\right)^3 \ln(\Lambda_f) \tag{A10}$$

and the stopping contribution from free electrons simplifies to [45]

$$S_f = \frac{4\pi Z_b^2 e^4 n_f}{m_e v_F^3} v_p \ln(\Lambda_f). \tag{A11}$$

In the limit of high projectile velocity, $v_p \gg v_{\mathrm{ave}}$, L_e becomes

$$L_e = \left(\frac{v_p}{v_r}\right)^3 \ln(\Lambda_f) \simeq \ln(\Lambda_f) \tag{A12}$$

and the stopping contribution from free electrons simplifies to [45]

$$S_f = \frac{4\pi Z_b^2 e^4}{m_e v_p^2} n_f \ln(\Lambda_f). \tag{A13}$$

Note that Eq. (A12) already gives a one percent accuracy for $v_p > 2v_{\mathrm{ave}}$.

APPENDIX B: SIMULATION OF STOPPING CONTRIBUTION FROM FREE ELECTRONS WITH THE LAPINS CODE

The statistic model used in the LAPINS code [53–56] to deal with the case that disregards degeneracy is based on the classical Boltzmann equation,

$$\frac{\partial f}{\partial t} + \boldsymbol{v}_k \cdot \frac{\partial f}{\partial \boldsymbol{r}} + q_k(\boldsymbol{E} + \boldsymbol{v}_k \times \boldsymbol{B}) \cdot \frac{\partial f}{\partial \boldsymbol{p}_t} = \left.\frac{\partial f}{\partial t}\right|_{\mathrm{coll}}, \tag{B1}$$

where the subscript k indicates the species of particles, $f = f(\boldsymbol{r}, \boldsymbol{p}, t)$ is the distribution function,

$\boldsymbol{r}$ is the position, $\boldsymbol{p}$ is the momentum, t is the time, $\boldsymbol{v}$ is the velocity, $\boldsymbol{E}$ is the electric field, $\boldsymbol{B}$ is the magnetic field, and the collision term $\partial f/\partial t|_{\mathrm{coll}}$ is the Boltzmann collision integral. On this occasion, the average energy of electrons is only determined by thermal temperature T and the quantum effect of electrons is completely not considered.

The model used in the LAPINS code to deal with degeneracy is based on the first principle Boltzmann-Uhling-Uhlenbeck (BUU) equation [57,72],

$$\frac{\partial f}{\partial t} + \boldsymbol{v}_k \cdot \frac{\partial f}{\partial \boldsymbol{r}} + q_k(\boldsymbol{E} + \boldsymbol{v}_k \times \boldsymbol{B}) \cdot \frac{\partial f}{\partial \boldsymbol{p}_t} = \left.\frac{\partial f}{\partial t}\right|_{\mathrm{coll}}^{\mathrm{BUU}}, \tag{B2}$$

where the BUU collisions can ensure that evolution of degenerate particles is enforced by the Pauli exclusion principle. This principle prevents degenerate particles from being scattered into an energy state that is already occupied.

In order to give the visual stopping contribution from free electrons per unit density, we do a series of simulations by the LAPINS code. The initial energy of proton beams is set to 1 MeV. The densities of the boron target are respectively ρ_s, $10\rho_s$, $100\rho_s$, $10^3\rho_s$, and $10^4\rho_s$, where ρ_s is the density of the solid boron target equal to 2.34 g/cm^3. The temperatures of the former three cases are set to be 1 eV, while the temperatures of the latter two are set to be 10 eV and 100 eV, respectively. The reason why a higher temperature is set for the last two cases is to avoid numerical errors in the integral due to the large degeneracy parameter Θ. In fact, when the density of the boron target is over 100 ρ_s, such changes of temperature will not influence the result a lot.

For each simulation, the density of the proton beam is set low enough to make sure the influence can be regarded as perturbations. Duration of the beam is set long enough to ensure that the beam is still being injected when the velocity of the protons in the front plane is slowed down to zero. As shown in Fig. 6(a), we can get the proton energy at any position in the target at any time. On this occasion, as is shown in Fig. 6(b), we can obtain the data of proton average energy E_{pi} as a function of distance in the deceleration process. We will then get the stopping contribution from free electrons of protons by $\delta E_{pi}/\delta z_i$. Dividing it by n, we can obtain the stopping contribution from free electrons per unit density S_e/n.

[1] L. Q. Xu, Y. Q. Chu, S. Y. Lin, E. Z. Li, T. F. Zhou, C. W. Mai, Y. H. Huang, Q. Zhang, B. Zhang, S. X. Wang *et al.*, Experimental study of core MHD events in thousand-second improved confinement plasma on the EAST tokamak, Nucl. Fusion **63**, 076007 (2023); G. Elizabeth, Nuclear-fusion reactor smashes energy record, Nature (London) **602**, 371 (2022); A. B. Zylstra, A. L. Kritcher, O. A. Hurricane, D. A. Callahan, K. Baker, T. Braun, D. T. Casey, D. Clark, K. Clark, T. Döppner, L. Divol, D. E. Hinkel, M. Hohenberger, C. Kong, O. L. Landen, A. Nikroo, A. Pak, P. Patel, J. E. Ralph, N. Rice, R. Tommasini, M. Schoff, M. Stadermann, D. Strozzi, C. Weber, C. Young, C. Wild, R. P. Town, and M. J. Edwards, Record energetics for an inertial fusion implosion at NIF, Phys. Rev. Lett. **126**, 025001 (2021).

[2] S. Y. Gus'kov, P. A. Kuchugov, and G. A. Vergunova, Extreme matter compression caused by radiation cooling effect in gigabar shock wave driven by laser-accelerated fast electrons, Matter Radiat. Extremes **6**, 020301 (2021).

[3] M. Liu, X. Ai, Y. Liu, Q. Chen, S. Zhang, Z. He, Y. Huang, and Q. Yin, Fabrication of solid CH-CD multilayer microspheres for inertial confinement fusion, Matter Radiat. Extremes **6**, 025901 (2021).

[4] V. T. Tikhonchuk, T. Gong, N. Jourdain, O. Renner, F. P. Condamine, K. Q. Pan, W. Nazarov, L. Hudec, J. Limpouch, R. Liska *et al.*, Studies of laser-plasma interaction physics with low-density targets for direct-drive inertial confinement fusion on the Shenguang III prototype, Matter Radiat. Extremes **6**, 025902 (2021).

[5] A. B. Zylstra, O. A. Hurricane, D. A. Callahan, A. L. Kritcher, J. E. Ralph, H. F. Robey, J. S. Ross, C. V. Young, K. L. Baker, D. T. Casey, T. Döppner, L. Divol, M. Hohenberger, S. L. Pape, A. Pak, P. K. Patel, R. Tommasini, S. J. Ali, P. A. Amendt, L. J. Atherton, B. Bachmann, D. Bailey, L. R. Benedetti, L. B. Hopkins, R. Betti, S. D. Bhandarkar, J. Biener, R. M. Bionta, N. W. Birge, E. J. Bond, D. K. Bradley, T. Braun, T. M. Briggs, M. W. Bruhn, P. M. Celliers, B. Chang, T. Chapman, H. Chen, C. Choate, A. R. Christopherson, D. S. Clark *et al.*, Burning plasma achieved in inertial fusion, Nature (London) **601**, 542 (2022).

[6] A. B. Zylstra, A. L. Kritcher, O. A. Hurricane, D. A. Callahan, J. E. Ralph, D. T. Casey, A. Pak, O. L. Landen, B. Bachmann, K. L. Baker, L. B. Hopkins, S. D. Bhandarkar, J. Biener, R. M. Bionta, N. W. Birge, T. Braun, T. M. Briggs, P. M. Celliers, H. Chen, C. Choate, D. S. Clark, L. Divol, T. Döppner, D. Fittinghoff, M. J. Edwards, M. G. Johnson, N. Gharibyan, S. Haan, K. D. Hahn, E. Hartouni, D. E. Hinkel, D. D. Ho, M. Hohenberger, J. P. Holder, H. Huang, N. Izumi, J. Jeet, O. Jones, S. M. Kerr, S. F. Khan, H. G. Kleinrath, V. G. Kleinrath, C. Kong, K. M. Lamb, S. L. Pape, N. C. Lemos, J. D. Lindl, B. J. Macgowan, A. J. Mackinnon, A. G. Macphee, E. V. Marley, K. Meaney, M. Millot, A. S. Moore, K. Newman, J. M. D. Nicola, A. Nikroo *et al.*, Experimental achievement and signatures of ignition at the National Ignition Facility, Phys. Rev. E **106**, 025202 (2022).

[7] S. Weber, Y. Wu, and J. Wang, Recent progress in atomic and molecular physics for controlled fusion and astrophysics, Matter Radiat. Extremes **6**, 023002 (2021).

[8] H. Hora, S. Eliezer, and N. Nissim, Elimination of secondary neutrons from laser proton-boron fusion, Laser Part. Beams **2021**, e13 (2021).

[9] X. Ribeyre, R. Capdessus, J. Wheeler, E. d'Humiéres, and G. Mourou, Multiscale study of high energy attosecond pulse interaction with matter and application to proton-Boron fusion, Sci. Rep. **12**, 4665 (2022).

[10] D. Margarone, J. Bonvalet, L. Giuffrida, A. Morace, V. Kantarelou, M. Tosca, D. Raffestin, P. Nicolai, A. Picciotto, Y. Abe *et al.*, In-target proton–boron nuclear fusion using a PW-class laser, Appl. Sci. **12**, 1444 (2022).

[11] C. Labaune, C. Baccou, S. Depierreux, C. Goyon, G. Loisel, V. Yahia, and J. Rafelski, Fusion reactions initiated by laser-accelerated particle beams in a laser-produced plasma, Nat. Commun. **4**, 2506 (2013).

[12] D. Hoffmann, R. Schneider, S. Wissink, and S. Hanna, Region of the 4-stars of C-12 studied with the capture reaction B-11 (P, gamma-3) C-12 (9.64 MeV), Bull. Am. Phys. Soc. **26**, 590 (1981).

[13] J. R. Calarco, J. Arruda-Neto, K. A. Griffioen, S. S. Hanna, D. H. H. Hoffmann, B. Neyer, R. E. Rand, K. Wienhard, and M. R. Yearian, Observation of monopole strength in the ^{12}C(e, e′p$_0$) ^{11}B reaction, Phys. Lett. B **146**, 179 (1984).

[14] R. G. Allas, S. S. Hanna, L. Meyer-Schützmeister, and R. E. Segel, Radiative capture of protons by B^{11} and the giant dipole resonance in C^{12}, Nucl. Phys. **58**, 122 (1964).

[15] R. E. Segel, S. S. Hanna, and R. G. Allas, States in C^{12} between 16.4 and 19.6 MeV, Phys. Rev. **139**, B818 (1965).

[16] L. Lamia, C. Spitaleri, V. Burjan, N. Carlin, S. Cherubini, V. Crucillà, M. G. Munhoz, M. G. Del Santo, M. Gulino, Z. Hons *et al.*, New measurement of the ^{11}B(p, α_0)^{8}Be bare-nucleus S(E) factor via the Trojan horse method, J. Phys. G: Nucl. Part. Phys. **39**, 015106 (2012).

[17] D. H. H. Hoffmann, A. Richter, G. Schrieder, and K. Seegebarth, Cross section for the reaction ^{12}C(e, p) ^{11}B; and its relevance to the formation of ^{11}B in active galaxies, Astrophys. J. **271**, 398 (1983).

[18] G. A. P. Cirrone, L. Manti, D. Margarone, G. Petringa, L. Giuffrida, A. Minopoli, A. Picciotto, G. Russo, F. Cammarata, P. Pisciotta *et al.*, First experimental proof of Proton Boron Capture Therapy (PBCT) to enhance protontherapy effectiveness, Sci. Rep. **8**, 1141 (2018); M. Roth, Fusion Day at GSI Darmstadt, 2022 (unpublished), Workshop_program.pdf (gsi.de).

[19] D. C. Moreau, Potentiality of the proton-boron fuel for controlled thermonuclear fusion, Nucl. Fusion **17**, 13 (1977).

[20] S. V. Putvinski, D. D. Ryutov, and P. N. Yushmanov, Fusion reactivity of the pB^{11} plasma revisited, Nucl. Fusion **59**, 076018 (2019).

[21] M. H. Sikora and H. R. Weller, A new evaluation of the ^{11}B(p, α)$\alpha\alpha$ reaction rates, J. Fusion Energy **35**, 538 (2016).

[22] T. A. Heltemes and G. A. Moses, BADGER v1. 0: A Fortran equation of state library, Comput. Phys. Commun. **183**, 2629 (2012).

[23] V. S. Belyaev, A. P. Matafonov, V. I. Vinogradov, V. P. Krainov, V. S. Lisitsa, A. S. Roussetski, G. N. Ignatyev, and V. P. Andrianov, Observation of neutronless fusion reactions in picosecond laser plasmas, Phys. Rev. E **72**, 026406 (2005).

[24] S. Kimura, A. Anzalone, and A. Bonasera, Comment on "Observation of neutronless fusion reactions in picosecond laser plasmas", Phys. Rev. E **79**, 038401 (2009).

[25] A. Picciotto, D. Margarone, A. Velyhan, P. Bellutti, J. Krasa, A. Szydlowsky, G. Bertuccio, Y. Shi, A. Mangione, J. E. Prokupek,

A. Malinowska, E. Krousky, J. Ullschmied, L. Laska, M. Kucharik, and G. Korn, Boron-proton nuclear-fusion enhancement induced in boron-doped silicon targets by low-contrast pulsed laser, Phys. Rev. X **4**, 031030 (2014).

[26] C. Baccou, S. Depierreux, V. Yahia, C. Neuville, C. Goyon, R. De Angelis, F. Consoli, J. E. Ducret, G. Boutoux, J. Rafelski *et al.*, New scheme to produce aneutronic fusion reactions by laser-accelerated ions, Laser Part. Beams **33**, 117 (2015).

[27] C. Labaune, C. Baccou, V. Yahia, C. Neuville, and J. Rafelski, Laser-initiated primary and secondary nuclear reactions in Boron-Nitride, Sci. Rep. **6**, 21202 (2016).

[28] L. Giuffrida, F. Belloni, D. Margarone, G. Petringa, G. Milluzzo, V. Scuderi, A. Velyhan, M. Rosinski, A. Picciotto, M. Kucharik, J. Dostal, R. Dudzak, J. Krasa, V. Istokskaia, R. Catalano, S. Tudisco, C. Verona, K. Jungwirth, P. Bellutti, G. Korn, and G. A. P. Cirrone, High-current stream of energetic α particles from laser-driven proton-boron fusion, Phys. Rev. E **101**, 013204 (2020).

[29] D. Margarone, A. Picciotto, A. Velyhan, J. Krasa, M. Kucharik, A. Mangione, A. Szydlowsky, A. Malinowska, G. Bertuccio, Y. Shi *et al.*, Advanced scheme for high-yield laser driven nuclear reactions, Plasma Phys. Control. Fusion **57**, 014030 (2015).

[30] J. Ren, Z. Deng, W. Qi, B. Chen, B. Ma, X. Wang, S. Yin, J. Feng, W. Liu, Z. Xu *et al.*, Observation of a high degree of stopping for laser-accelerated intense proton beams in dense ionized matter, Nat. Commun. **11**, 5157 (2020).

[31] J. Bonvalet, P. Nicolaï, D. Raffestin, E. D'humieres, D. Batani, V. Tikhonchuk, V. Kantarelou, L. Giuffrida, M. Tosca, G. Korn *et al.*, Energetic α-particle sources produced through proton-boron reactions by high-energy high-intensity laser beams, Phys. Rev. E **103**, 053202 (2021).

[32] K.-F. Liu and A. W. Chao, Accelerator based fusion reactor, Nucl. Fusion **57**, 084002 (2017).

[33] G. Zwicknagel, C. Toepffer, and P.-G. Reinhard, Stopping of heavy ions in plasmas at strong coupling, Phys. Rep. **309**, 117 (1999).

[34] A. C. Hayes, M. E. Gooden, E. Henry, G. Jungman, J. B. Wilhelmy, R. S. Rundberg, C. Yeamans, G. Kyrala, C. Cerjan, D. L. Danielson, J. Daligault, C. Wilburn, P. Volegov, C. Wilde, S. Batha, T. Bredeweg, J. L. Kline, G. P. Grim, E. P. Hartouni, D. Shaughnessy, C. Velsko, W. S. Cassata, K. Moody, L. F. Berzak Hopkins, D. Hinkel, T. Döppner, S. Le Pape, F. Graziani, D. A. Callahan, O. A. Hurricane, and D. Schneider, Plasma stopping-power measurements reveal transition from non-degenerate to degenerate plasmas, Nat. Phys. **16**, 432 (2020).

[35] X. C. Ning, T. Y. Liang, D. Wu, S. J. Liu, Y. C. Liu, T. X. Hu, Z. M. Sheng, J. R. Ren, B. W. Jiang, Y. T. Zhao, D. H. H. Hoffmann, X. T. He *et al.*, Laser-driven proton-boron fusions: Influences of the boron state, Laser Part. Beams **2022**, e8 (2022).

[36] S. Atzeni and J. Meyer-ter-Vehn, *The Physics of Inertial Fusion: Beam Plasma Interaction, Hydrodynamics, Hot Dense Matter* (Oxford University Press, Oxford, 2004), Vol. 125.

[37] K. T. Lorenz, M. J. Edwards, A. F. Jankowski, S. M. Pollaine, R. F. Smith, and B. A. Remington, High pressure, quasi-isentropic compression experiments on the Omega laser, High Energy Density Phys. **2**, 113 (2006).

[38] G. Ghisellini, Bremsstrahlung and Black Body, in *Radiative Processes in High Energy Astrophysics*, Lecture Notes in Physics, Vol. 873 (Springer International Publishing, Heidelberg, 2013), pp. 23–29.

[39] S. Skupsky, Energy loss of ions moving through high-density matter, Phys. Rev. A **16**, 727 (1977).

[40] U. Fano, Penetration of protons, alpha particles, and mesons, Annu. Rev. Nucl. Sci. **13**, 1 (1963).

[41] C. F. Clauser and N. R. Arista, Stopping power of dense plasmas: The collisional method and limitations of the dielectric formalism, Phys. Rev. E **97**, 023202 (2018).

[42] P. Sigmund, Kinetic theory of particle stopping in a medium with internal motion, Phys. Rev. A **26**, 2497 (1982).

[43] N. R. Arista and P. Sigmund, Stopping of ions based on semiclassical phase shifts, Phys. Rev. A **76**, 062902 (2007).

[44] C. F. Clauser and N. R. Arista, Energy loss and Z oscillations of atomic beams in plasmas, Phys. Rev. E **88**, 053102 (2013).

[45] J. M. Fernández-Varea and N. R. Arista, Analytical formula for the stopping power of low-energy ions in a free-electron gas, Radiat. Phys. Chem. **96**, 88 (2014).

[46] S. Son and N. J. Fisch, Aneutronic fusion in a degenerate plasma, Phys. Lett. A **329**, 76 (2004).

[47] J. Lindhard and A. Winther, Stopping power of electron gas and equipartition rule, Mat. Fys. Medd. Dan. Vid. Selsk. **34**, 4 (1964).

[48] G. Maynard and C. Deutsch, Energy loss and straggling of ions with any velocity in dense plasmas at any temperature, Phys. Rev. A **26**, 665 (1982).

[49] G. Maynard and C. Deutsch, Born random phase approximation for ion stopping in an arbitrarily degenerate electron fluid, J. Phys. **46**, 1113 (1985).

[50] C. Deutsch and G. Maynard, Ion stopping in dense plasmas: A basic physics approach, Matter Radiat. Extremes **1**, 277 (2016).

[51] T.-X. Hu, J.-H. Liang, Z.-M. Sheng, and D. Wu, Kinetic investigations of nonlinear electrostatic excitations in quantum plasmas, Phys. Rev. E **105**, 065203 (2022).

[52] G. F. Bertsch and S. D. Gupta, A guide to microscopic models for intermediate energy heavy ion collisions, Phys. Rep. **160**, 189 (1988).

[53] D. Wu, W. Yu, S. Fritzsche, and X. T. He, High-order implicit particle-in-cell method for plasma simulations at solid densities, Phys. Rev. E **100**, 013207 (2019).

[54] D. Wu, X. T. He, W. Yu, and S. Fritzsche, Monte Carlo approach to calculate proton stopping in warm dense matter within particle-in-cell simulations, Phys. Rev. E **95**, 023207 (2017).

[55] D. Wu, Z. M. Sheng, W. Yu, S. Fritzsche, and X. T. He, A pairwise nuclear fusion algorithm for particle-in-cell simulations: Weighted particles at relativistic energies, AIP Adv. **11**, 075003 (2021).

[56] D. Wu, W. Yu, Y. T. Zhao, D. H. H. Hoffmann, S. Fritzsche, and X. T. He, Particle-in-cell simulation of transport and energy deposition of intense proton beams in solid-state materials, Phys. Rev. E **100**, 013208 (2019).

[57] D. Wu, W. Yu, S. Fritzsche, and X. T. He, Particle-in-cell simulation method for macroscopic degenerate plasmas, Phys. Rev. E **102**, 033312 (2020).

[58] R. Cabrera-Trujillo, S. A. Cruz, J. Oddershede, and J. R. Sabin, Bethe theory of stopping incorporating electronic excitations of partially stripped projectiles, Phys. Rev. A **55**, 2864 (1997).

[59] J. M. Gil, P. R. Beltrán, R. Rodríguez, G. Espinosa, M. D. Barriga-Carrasco, and L. González-Gallego, Bound electron stopping power model of partially stripped ions in partially ionized plasmas, X-Ray Spectrom. **49**, 234 (2020).

[60] F. B. Rosmej, V. A. Astapenko, and V. S. Lisitsa, *Plasma Atomic Physics*, Springer Series on Atomic, Optical, and Plasma Physics, Vol. 104 (Springer, Berlin, 2021).

[61] S. X. Hu, Continuum lowering and Fermi-surface rising in strongly coupled and degenerate plasmas, Phys. Rev. Lett. **119**, 065001 (2017).

[62] T. A. Mehlhorn, A finite material temperature model for ion energy deposition in ion-driven inertial confinement fusion targets, J. Appl. Phys. **52**, 6522 (1981).

[63] O. Ciricosta, S. M. Vinko, H.-K. Chung, B.-I. Cho, C. R. D. Brown, T. Burian, J. Chalupský, K. Engelhorn, R. W. Falcone, C. Graves, V. Ha'jkova', A. Higginbotham, L. Juha, J. Krzywinski, H. J. Lee, M. Messerschmidt, C. D. Murphy, Y. Ping, D. S. Rackstraw, A. Scherz, W. Schlotter, S. Toleikis, J. J. Turner, L. Vysin, T. Wang, B. Wu, U. Zastrau, D. Zhu, R. W. Lee, P. Heimann, B. Nagler, and J. S. Wark, Direct measurements of the ionization potential depression in a dense plasma, Phys. Rev. Lett. **109**, 065002 (2012).

[64] P. Sigmund, *Particle Penetration and Radiation Effects Volume 2: Penetration of Atomic and Molecular Ions*, Springer Series in Solid-State Sciences (Springer, Berlin, 2014), Vol. 179.

[65] C. E. Starrett, Coulomb log for conductivity of dense plasmas, Phys. Plasmas **25**, 092707 (2018).

[66] F. Belloni and K. Batani, Multiplication processes in high-density H-^{11}B fusion fuel, Laser Part. Beams **2022**, e11 (2022).

[67] L. Robson, P. T. Simpson, R. J. Clarke, K. W. D. Ledingham, F. Lindau, O. Lundh, T. McCanny, P. Mora, D. Neely, C.-G. Wahlström, M. Zepf, and P. McKenna, Scaling of proton acceleration driven by petawatt-laser-plasma interactions, Nat. Phys. **3**, 58 (2007).

[68] D. S. Hey, M. E. Foord, M. H. Key, S. L. LePape, A. J. Mackinnon, P. K. Patel, Y. Ping, K. U. Akli, R. B. Stephens, T. Bartal, F. N. Beg, R. Fedosejevs, H. Friesen, H. F. Tiedje, and Y. Y. Tsui, Laser-accelerated proton conversion efficiency thickness scaling, Phys. Plasmas **16**, 123108 (2009).

[69] M. Mehrangiz, A. Ghasemizad, S. Jafari, and B. Khanbabaei, Fusion energy and stopping power in a degenerate DT pellet driven by a laser-accelerated proton beam, Commun. Theor. Phys. **65**, 761 (2016).

[70] R. C. Davidson, M. A. Dorf, I. D. Kaganovich, H. Qin, A. Sefkow, E. A. Startsev, D. R. Welch, D. V. Rose, and S. M. Lund, Survey of collective instabilities and beam–plasma interactions in intense heavy ion beams, Nucl. Instrum. Methods Phys. Res. Sect. A **606**, 11 (2009).

[71] R. Betti, A. A. Solodov, J. A. Delettrez, and C. Zhou, Gain curves for direct-drive fast ignition at densities around $300 g/cc$, Phys. Plasmas **13**, 100703 (2006).

[72] A. Domps, P.-G. Reinhard, and E. Suraud, Fermionic Vlasov propagation for Coulomb interacting systems, Ann. Phys. (NY) **260**, 171 (1997).